Jurnal Ilmu Fisika
Vol. 18, No. 2, September 2026, pp. 117–128
ISSN: 1979-4657 (Print); 2614-7386 (Online)
https://doi.org/10.25077/jif.18.2.117-128.2026

Jurnal Ilmu Fisika
Open Access

Thermodynamic Analysis of an Endoreversible Bosonic Quantum Otto Refrigerator under Partial Thermalization

Shofiyah Shofiyah, Trengginas Eka Putra Sutantyo*, Zulfi Abdullah

Theoretical Physics Laboratory, Department of Physics, Faculty of Mathematics and Natural Sciences, Universitas Andalas, Limau Manis, Padang, 25163, Indonesia

Article Info

Article History:

Received December 08, 2025
Revised March 18, 2026
Accepted April 18, 2026
Published online April 24, 2026

Keywords:

Coefficient of Performance (COP)
Cubic Potential
Otto Cycle
Partial Thermalization
Quantum Refrigerator

Corresponding Author:

Trengginas E. P. Sutantyo,
Email:
trengginasekaputra@sci.unand.ac.id

ABSTRACT

Quantum refrigerators (QRs) are pivotal in exploring thermodynamic behavior at microscopic scales. This study investigates a quantum Otto refrigerator using a bosonic gas confined in a cubic potential, operating under finite-time thermalization. We derive key thermodynamic quantities analytically, including the coefficient of performance (COP), cooling power, entropy, and cooling rate. Additionally, we investigate how partial thermalization during the isochoric heating and cooling stages influences overall system performance. The findings reveal a trade-off between COP and cooling power, emphasizing the importance of thermalization duration. Notably, by extending the cooling time relative to heating, the COP can be significantly improved, offering a practical approach to optimizing QR performance under realistic conditions.

1. INTRODUCTION

The increasing demand for efficient cooling technologies in cryogenics, quantum technologies, and high-precision detection highlights the limitations of conventional refrigeration systems. These systems typically rely on synthetic refrigerants such as chlorofluorocarbons (CFCs) and hydrofluorocarbons (HFCs), which contribute to ozone depletion and global warming (Mohapatra et al., 2021; Mohanraj & Abraham, 2022; Savitha et al., 2022). Moreover, classical refrigeration methods are not optimized for microscale applications, where precise thermal management is essential. In quantum computing and sensing, even minor thermal fluctuations can compromise coherence and system stability (Myers et al., 2022b; Cleri, 2024).

The study of energy transfer in quantum systems has led to the development of quantum thermodynamics, notably since Scovil and Schulz-DuBois introduced quantum engines in the 1950s. Various quantum thermal models have been proposed, such as Otto (Nolte, 2019; Abah et al., 2020; T. Sutantyo, 2020; Jiao et al., 2021; Wiedmann et al., 2021; V. Singh et al., 2022; Behzadi, 2024; Kaur et al., 2025), Carnot (Belfaqih et al., 2015; Kurniasih et al., 2019; Fei et al., 2022; Z. Zhang et al., 2023; Contreras-Vergara et al., 2024; Altintas, 2025; He et al., 2025), and Stirling (Yin et al., 2017; Getie et

al., 2020; Raja et al., 2021; Cruz et al., 2023), to explore thermodynamic limits at the microscale (Maslennikov et al., 2019; Manikandan et al., 2020; Bhandari & Jordan, 2021; Fahriza et al., 2022). The quantum Otto cycle, in particular, has gained attention for its simplicity and effectiveness in modeling energy conversion in finite systems (Chen et al., 2019, 2021). When configured as a quantum refrigerator, it aims to extract maximum heat from a cold reservoir with minimal external work input. Its performance is typically assessed using the coefficient of performance (COP) and cooling power (Camati et al., 2020)

A central challenge in quantum refrigeration lies in enhancing the COP without sacrificing cooling power. Although the maximum COP is theoretically achieved in the quasistatic limit, such operation requires infinitely slow cycles and consequently yields negligible cooling power. Practical implementations necessarily operate in the finite-time regime, where dissipation and entropy production reduce overall efficiency (Abah et al., 2020; Jiao et al., 2021). Unlike heat engines, often optimized for maximum power, quantum refrigerators lack a universal optimization framework. Consequently, current research focuses on balancing the COP and cooling rate to assess and improve performance under realistic operating conditions.

Recent studies have examined quantum Otto refrigerators under partial thermalization to account for finite reservoir contact times (Abah et al., 2020; Y. Zhang, 2020; T. E. P. Sutantyo et al., 2024; Xu et al., 2025). However, most existing models employ low-dimensional working media such as qubits or particles confined in harmonic traps and rarely consider explicit three-dimensional spatial confinement (Long & Liu, 2015; S. Singh & Abah, 2020). In harmonic models, compression and expansion are implemented through variations of the trap frequency, meaning that the working parameter is dynamical rather than geometric. Consequently, changes in the cycle do not directly correspond to physical volume deformation of the system.

To address this limitation, the present study investigates a quantum Otto refrigerator with a non-interacting Bose gas confined in a three-dimensional cubic potential. The non-interacting bosonic model is chosen because it allows analytical derivation of thermodynamic quantities while retaining essential quantum statistical features (Bagnato et al., 1987; Pathria & Beale, 2011a). In contrast to harmonic confinement, cubic confinement provides a well-defined spatial boundary with an explicit system volume. The energy spectrum depends directly on the geometric size of the cube, such that variations in the side length modify the energy levels and density of states through geometric scaling. Therefore, compression and expansion in this configuration correspond to genuine physical volume changes of the system.

To represent realistic operating conditions, partial thermalization is incorporated within an endoreversible framework, where irreversibility arises solely from finite-time heat exchange with the reservoirs. This approach enables closed-form analytical expressions for the principal performance metrics, although internal dissipation, particle interactions, and control imperfections are neglected. The thermodynamic performance is evaluated through the coefficient of performance (COP), cooling rate, output power, and entropy production, providing a comprehensive assessment of how bosonic statistics, cubic geometry, and finite-time thermalization influence the behavior of a quantum Otto refrigerator.

2. THERMODYNAMIC PROPERTIES OF BEC

An ideal Bose gas confined in a three-dimensional cubic potential is employed as the working medium of the quantum Otto refrigerator. In contrast to the commonly used harmonic confinement, cubic confinement possesses well-defined spatial boundaries and an explicit system volume. This allows a direct examination of how geometric scaling influences the energy spectrum and thermodynamic properties (Belfaqih et al., 2015; T. E. P. Sutantyo et al., 2015). The cubic potential is treated as the limiting case of a general power-law trapping potential (Zettili, 2009; Griffiths & Schroeter, 2018; T. E. P. Sutantyo et al., 2024), formulated as:

$$\mathcal{V}(x,y,z) = \mathcal{V}(r) = \varepsilon_0 \left(\left|\frac{x}{a}\right|^p + \left|\frac{y}{b}\right|^q + \left|\frac{z}{c}\right|^l \right) \tag{1}$$

By setting $a = b = c$ and $p = q = l \to \infty$, the general power-law potential approaches a three-dimensional box confinement in which the potential remains finite inside the domain and rises steeply at the boundaries, effectively forming rigid walls (T. E. P. Sutantyo et al., 2024). In this limiting representation, the system behaves as particles confined in a cubic box with well-defined boundary conditions. This configuration permits an analytical formulation of the density of states and the thermodynamic quantities of the system. The system is analyzed within the grand canonical ensemble, which is appropriate for describing a Bose gas at low temperatures. In this framework, the grand potential is expressed as:

$$\Omega = k_B T \sum_i \ln\left(1 - z e^{-\beta \varepsilon_i}\right), \tag{2}$$

where $\beta = 1/k_B T$, and $z = e^{\mu/k_B T}$ is the fugacity. Bose–Einstein condensation (BEC) occurs when the chemical potential $\mu \to 0$, such that below the critical temperature a macroscopic fraction of particles occupies the ground state.

$$T_c = \frac{2\pi\hbar^2}{m k_B}\left(\frac{1}{\zeta(3/2)}\frac{N}{V}\right)^{\frac{2}{3}}, \tag{3}$$

with $\zeta(3/2) \approx 2.612$ is the Riemann zeta function. Here, the rubidium-87 atoms with $N/V = 1.5 \times 10^{19}\,\mathrm{m}^{-3}$ and $m = 1.419 \times 10^{-25}\,\mathrm{kg}$ are utilized as a bosonic gas, which yields a critical temperature of approximately $T_c = 130\,\mathrm{nK}$ (Aveline et al., 2020). At temperatures lower than this threshold, the gas undergoes the BEC phase, where most particles occupy the ground state. In this regime, the thermodynamic properties of the system can be described analytically through the Maxwell relation (Pathria & Beale, 2011b). The entropy is given by:

$$S(T,V) = \frac{5}{2} k_B V \left(\frac{m k_B T}{2\pi\hbar^2}\right)^{\frac{3}{2}} g_{5/2}(1), \tag{4}$$

and the number of thermally excited particles is (Bagnato et al., 1987; Hu et al., 2021; Myers et al., 2022a):

$$N_T = V\left(\frac{m k_B T}{2\pi\hbar^2}\right)^{3/2} g_{3/2}(z). \tag{5}$$

Meanwhile, the internal energy is obtained using the thermodynamic identity. $U = \Omega + TS + \mu N$,

$$U(T,V) = \frac{3}{2} k_B T V \left(\frac{m k_B T}{2\pi\hbar^2}\right)^{3/2} g_{5/2}(1), \tag{6}$$

All these thermodynamic parameters are expressed in terms of the Boson function, defined as:

$$g_\nu(z) = \sum_{n=1}^{\infty} \frac{z^n}{n^\nu} \tag{7}$$

which converges for $z < 1$, and can be extended to $z = 1$ using the Riemann zeta function $\zeta(\nu)$ (Pathria & Beale, 2011b).

3. THE ENDOREVERSIBLE QUANTUM OTTO REFRIGERATOR

The quantum Otto refrigerator functions as the reversed counterpart of the quantum Otto heat engine cycle. As illustrated in Figure 1, the cycle consists of four sequential thermodynamic processes forming a full cycle: isentropic compression (1→2), isochoric heating (2→3), isentropic expansion (3

→4), and isochoric cooling (4→1). In the classical Otto engine, compression and expansion are performed mechanically via the motion of a piston. In contrast, quantum systems implement these transformations by modulating the external trapping potential, which effectively alters the system's accessible volume. During the isochoric strokes, the external potential remains constant, allowing thermal interaction with a reservoir. Conversely, throughout the isentropic strokes, the potential is varied gradually while the system is kept isolated to ensure adiabatic evolution. To account for finite-time operation and associated irreversibility, we employ the endoreversible thermodynamic framework (Curzon & Ahlborn, 1975; Myers et al., 2022a; T. E. P. Sutantyo et al., 2024) in this study. Within this framework, the working medium is assumed to remain in local equilibrium during isentropic strokes. At the same time, incomplete thermalization occurs during the isochoric strokes due to unequal stroke time with the reservoirs. In this study, the adopted sign convention takes the work performed by the working medium during expansion as positive, $W_{\mathrm{exp}} > 0$, whereas the work done on the system during compression is negative, $W_{\mathrm{com}} < 0$. Accordingly, in the refrigeration cycle, the heat absorbed by the working medium from the low-temperature reservoir is taken as positive, $Q_{\mathrm{in}} > 0$, while the heat released by the system into high-temperature reservoir is negative, $Q_{\mathrm{out}} < 0$, as shown in Figure 1.

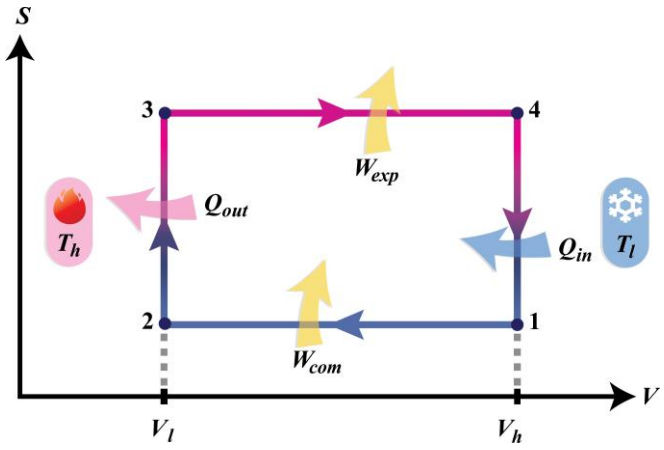

Figure 1 Entropy (*S*) vs Volume (*V*) diagram of the quantum Otto refrigerator.

3.1 Isentropic Compression (1 → 2)

During isentropic compression, the system is isolated from the environment, so no heat is exchanged. $\Delta Q = 0$. Thus, according to the First Law of Thermodynamics, the work performed during compression ($W_{comp} < 0$) is obtained from the difference in internal energy given by Eq. (6).

$$W_{comp} = U(T_2, V_l) - U(T_1, V_h) = \frac{3}{2} k_B \left(\frac{m k_B}{2\pi\hbar^2}\right)^{3/2} \left(T_2^{5/2} V_l - T_1^{5/2} V_h\right) g_{5/2}(1) \tag{8}$$

Moreover, from the entropy conservation in this process $\Delta S = 0$, we obtain the relation:

$$T_2 = T_1 \left(\frac{V_h}{V_l}\right)^{2/3}, \tag{9}$$

and by defining κ as:

$$\kappa = \frac{V_h}{V_l} \tag{10}$$

We rewrite the work as:

$$W_{comp} = \frac{3}{2} k_B \left(\frac{mk_B}{2\pi\hbar^2}\right)^{3/2} T_1^{5/2} V_l \left(\kappa^{5/3} - \kappa\right) g_{5/2}(1). \tag{11}$$

3.2 Isochoric Heating (2 → 3)

This process occurs at constant volume V_l, so the work done is zero, and the energy change arises from heat flowing out ($Q_{out} < 0$)

$$Q_h = U(T_3, V_l) - U(T_2, V_l) = \frac{3}{2} k_B \left(\frac{mk_B}{2\pi\hbar^2}\right)^{3/2} V_l \left(T_3^{5/2} - T_2^{5/2}\right) g_{5/2}(1). \tag{12}$$

In this study, the thermalization of the working medium is formulated using Fourier's law (Deffner & Campbell, 2019; Myers et al., 2022a; Zettira et al., 2024a, 2024b), reflecting the heat flow driven by temperature differences between the reservoir and system,

$$\frac{dT}{dt} = -\alpha_h (T - T_h). \tag{13}$$

With the boundary condition $T(0) = T_2$, $T(\tau_h) = T_3$ the solution becomes:

$$T_3 - T_h = (T_2 - T_h) e^{-\alpha_h \tau_h} \tag{14}$$

3.3 Isentropic Expansion (3 → 4)

During this stroke, no heat exchange occurs. The work done ($W_{exp} > 0$) in this expansion process is:

$$W_{exp} = U(T_4, V_h) - U(T_3, V_l) = \frac{3}{2} k_B \left(\frac{mk_B}{2\pi\hbar^2}\right)^{3/2} \left(T_4^{5/2} V_h - T_3^{5/2} V_l\right) g_{5/2}(1). \tag{15}$$

From the entropy conservation and relation in Eq. (10), we gain:

$$T_3 = T_4 \kappa^{2/3}. \tag{16}$$

Substituting into the work expression in Eq. (15), we rewrite the work as follows:

$$W_{exp} = \frac{3}{2} k_B \left(\frac{mk_B}{2\pi\hbar^2}\right)^{3/2} T_4^{5/2} V_l \left(\kappa - \kappa^{5/3}\right) g_{5/2}(1) \tag{17}$$

3.4 Isochoric Cooling (4 → 1)

Similar to the previous isochoric process, this process occurs at constant volume V_h. The heat flowing in ($Q_{in} > 0$) from the cold reservoir during the isochoric cooling stroke is defined as the change in internal energy of the working medium from state 4 to state 1, namely:

$$Q_l = U(T_1, V_h) - U(T_4, V_h) = \frac{3}{2} k_B \left(\frac{mk_B}{2\pi\hbar^2}\right)^{3/2} V_h \left(T_1^{5/2} - T_4^{5/2}\right) g_{5/2}(1). \tag{18}$$

This heat flow is driven by temperature differences during the thermalization process, which is stated as:

$$T_1 - T_l = (T_4 - T_l) e^{-\alpha_l \tau_l} \tag{19}$$

4. RESULT AND DISCUSSION

4.1 Coefficient of Performance

The Coefficient of Performance (COP), denoted by ε, serves as a key metric for evaluating the performance of refrigeration systems. It is defined as the ratio between the amount of heat absorbed from the cold reservoir and the total work required to complete one thermodynamic cycle (Çengel, 2008; Abah et al., 2020).

$$\varepsilon = \frac{Q_l}{W_{net}} = \frac{Q_l}{Q_h - Q_l} \tag{20}$$

By substituting Eq. (12) and (18), the explicit expression for the COP is obtained as follows:

$$\varepsilon = \frac{1}{k^{2/3} - 1} \tag{21}$$

Under such ideal conditions, the COP approaches its thermodynamically permitted upper bound, given by the Carnot limit $\varepsilon_C = \frac{T_l}{T_h - T_l}$ (Velasco et al., 1997; Abah & Lutz, 2016), where T_l and T_h are the temperatures of the cold and hot reservoirs, respectively. The value of ε_c represents the theoretical upper bound of efficiency for a reversible refrigeration system operating between these two reservoir temperatures. However, in practical applications, the actual COP will always be lower than ε_C due to dissipative effects and thermal imbalance.

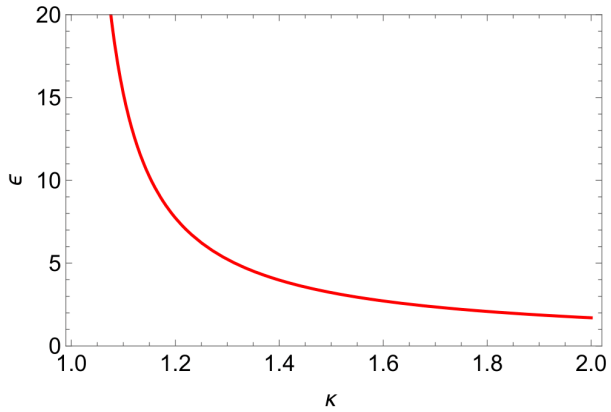

Figure 2 The coefficient of performance ε as a function of the volume ratio $\kappa = V_h/V_l$

Furthermore, as shown in Fig. (2), the COP decreases dramatically as κ increases, especially when $\kappa > 1$. This reduction is attributed to the increase in net work W_{net} required to complete the cycle, due to the enhanced expansion volume and elevated final temperature. In other words, the system demands greater energy input to extract the same amount of heat from the cold reservoir. Although larger values of κ may accelerate the cooling cycle, this comes at the expense of increased energy dissipation and significant irreversible entropy production.

This phenomenon indicates that the system has entered the non-quasistatic regime, wherein complete thermal equilibrium is no longer achieved during the cycle. It exemplifies the classical trade-off between efficiency and cooling power, as established by the framework of finite-time thermodynamics. High efficiency requires slow processes, while high cooling power relies on faster dynamics, which result in reduced efficiency. As demonstrated in Figure 2, the COP decreases monotonically with increasing κ, with a steep decline observed for $\kappa > 1.5$. This highlights the importance of selecting an optimal value of κ, one that is sufficiently high to sustain adequate cooling power but not excessively large, so as to avoid a drastic degradation in efficiency. Therefore, in designing quantum Otto-based refrigeration systems, controlling the trap geometry (volume ratio) and thermalization duration becomes a key strategy for achieving optimal thermodynamic performance under realistic operating time constraints.

4.2 Power

The output power (P) of the quantum Otto refrigerator is defined as the total net work per cycle divided by the total cycle time. In this model, the total duration of the cycle is dominated by the two isochoric processes, heating and cooling, which take finite times τ_h and τ_l, respectively. The power output is (Myers et al., 2022a):

$$P = -\frac{W_{net}}{\tau}, \tag{22}$$

The magnitude of work performed during the compression process (W_{comp}) and expansion process (W_{exp}). Within this framework, the system temperatures at the transition points between isentropic and isochoric processes, namely T_1 and T_4, are not directly assumed to be identical to the reservoir temperatures. Instead, temperature evolution follows a modified version of Fourier's law adapted for finite-time interactions (Bagnato et al., 1987; Myers et al., 2022a; T. E. P. Sutantyo et al., 2024). Based on the exponential solution of linear differential equations, the following expressions are obtained:

$$T_1 = \frac{\kappa^{2/3}(e^{\alpha_l \tau_l} - 1)T_l + (1 - e^{-\alpha_h \tau_h})T_h}{\kappa^{2/3}(e^{\alpha_l \tau_l} - e^{-\alpha_h \tau_h})}, \tag{23}$$

and

$$T_4 = \frac{(e^{\alpha_h \tau_h} - 1)T_h + \kappa^{2/3}(1 - e^{-\alpha_l \tau_l})T_l}{\kappa^{2/3}(e^{\alpha_h \tau_h} - e^{-\alpha_l \tau_l})}, \tag{24}$$

α_l, α_h are the heat transfer coefficients during isochoric interaction with the cold and hot reservoirs, respectively. By substituting T_1 and T_4 into the internal energy expressions, and combining them in the isentropic work terms, the output power per cycle can be expressed as

$$P = \frac{\frac{3}{2}k_B V_l \left(\frac{mk_B}{2\pi\hbar^2}\right)^{3/2} \zeta\left(\frac{5}{2}\right)}{\gamma(\tau_h + \tau_L)(1+\varepsilon)^{5/2}(e^{\alpha_l\tau_l + \alpha_h\tau_h} - 1)^{5/2}} \left\{\left[T_l\left(\frac{1}{\varepsilon} + 1\right)e^{\alpha_h\tau_h}(e^{\alpha_l\tau_l} - 1) + T_h(e^{\alpha_h\tau_h} - 1)\right]^{5/2} - \left[T_h e^{\alpha_l\tau_l}(e^{\alpha_h\tau_h} - 1) + T_l\left(\frac{1}{\varepsilon} + 1\right)(e^{\alpha_l\tau_l} - 1)\right]^{5/2}\right\} \tag{25}$$

Figure 3 illustrates how the combination of hot (τ_h) and cold (τ_l) thermalization durations influence the dimensionless output power (P^*) as a function of COP (ε). In the slow symmetric configuration ($\tau_h = \tau_l = 10$, blue curve), the output power reaches its minimum. This observation is consistent with the principle that systems operating in the quasistatic limit exhibit high efficiency but very low power, due to extended cycle times.

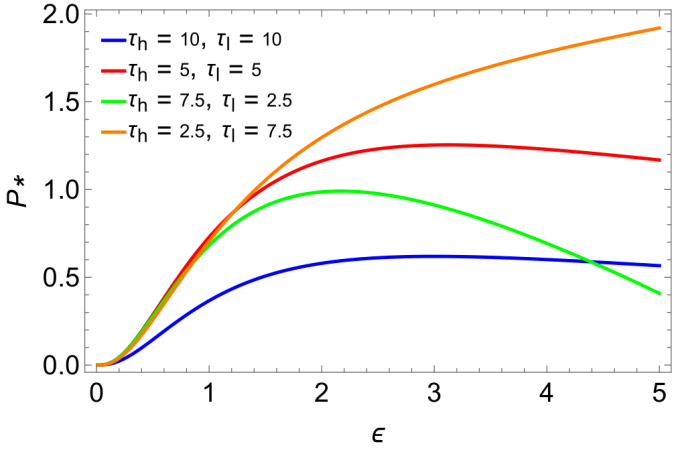

Figure 3 The dimensionless power output (P^*) versus the COP (ε) for a quantum Otto refrigerator with various time strokes.

When the duration of the cycle is reduced to the same thermalization time ($\tau_h = \tau_l = 5$, red curve), the power increases significantly. This shows that shortening the cycle duration enhances output power, although with the drawback of imperfect thermalization and increased irreversibility. Here, the

classical quantum trade-off emerges: power rises while entropy production also increases. This balance lies at the core of finite-time quantum thermodynamics. However, the most notable observation arises from the asymmetric configuration, i.e., partial thermalization. In the green curve ($\tau_h = 7.5, \tau_l = 2.5$), the power is lower than in the fast-symmetric case, despite identical total cycle durations. This implies that prolonged heating and insufficient cooling are detrimental. The underlying reason is that the system does not receive adequate time to absorb heat efficiently from the cold reservoir, whereas more energy is wasted during prolonged interaction with the highly entropic hot reservoir.

Conversely, the orange curve ($\tau_h = 2.5, \tau_l = 7.5$) yields the maximum output power. This outcome is aligned with quantum thermodynamic principles, wherein extended interaction with the statistically "ordered" cold reservoir allows more efficient heat extraction, and brief heating minimizes dissipation from the hot reservoir. This constitutes optimal entropy management, extending the more productive cooling stage while compressing the more dissipative heating stage. Overall, the graph confirms that partial thermalization timing constitutes one of the most effective control mechanisms in quantum refrigeration systems. It is not sufficient to merely optimize reservoir temperatures and trap volumes; to maximize output power, system designers must consider cycle timing strategies that target critical points within the energy and dissipation dynamics.

4.3 Cooling Rate

The cooling rate (R) is defined as the amount of heat extracted from the cold reservoir, Q_l, divided by the total duration of the thermodynamic cycle (Long & Liu, 2015; Abah et al., 2020). This metric is analogous to output power, but with a specific emphasis on the system's cooling capability. Mathematically, it can be expressed as

$$R = \frac{Q_l}{\tau} = \frac{Q_l}{\gamma(\tau_h + \tau_l)}, \tag{26}$$

where γ is a time-scaling factor, and τ_h , τ_l denote the thermalization times during isochoric interaction with the hot and cold reservoirs, respectively. In this model, the heat absorbed from the cold reservoir is derived from the change in internal energy during the isochoric cooling process at low volume (V_l). The internal energy of the working medium scales with temperature as $U \propto T^{5/2}$. Accordingly, the cooling power can be expressed as:

$$R = \frac{\frac{3}{2} k_B \left(\frac{m k_B}{2\pi\hbar^2}\right)^{3/2} g_{5/2}(1) V_h (T_1 - T_4)^{5/2}}{\gamma(\tau_h + \tau_l)}, \tag{27}$$

with T_1 and T_4 obtained from partial thermalization based on exponential Fourier dynamics (T. E. P. Sutantyo et al., 2024). Figure 4 illustrates the cooling rate (R) versus COP (ε)across six thermalization-time configurations. All curves show a decreasing trend, highlighting the fundamental quantum thermodynamic trade-off: higher efficiency requires sacrificing cooling power. Case A ($\tau_h = 10, \tau_l = 10$) provides the highest R at low (ε), benefiting from extended thermal contact. In contrast, Case F ($\tau_h = 2.5, \tau_l = 2.5$) yields consistently low performance, suggesting insufficient thermalization. Comparing Cases C and D, both with equal cycle times but opposite asymmetry, reveals that longer heating ($\tau_h = 7.5$) improves R, underscoring the dominant influence of hot-reservoir interaction. Cases B and E, with symmetric but shorter durations, offer intermediate results, emphasizing that total contact time is as crucial as its distribution.

4.4 Entropy Change of Working Medium

The entropy change of the working medium during the isochoric processes, which represents the entropy of bosonic gas in finite-time operation, is given in Eqs. (28)–(29). Within the endoreversible framework, the total entropy production over one cycle is defined as the sum of the entropy changes of the working medium and the reservoirs, and it remains non-negative (Altintas, 2025).

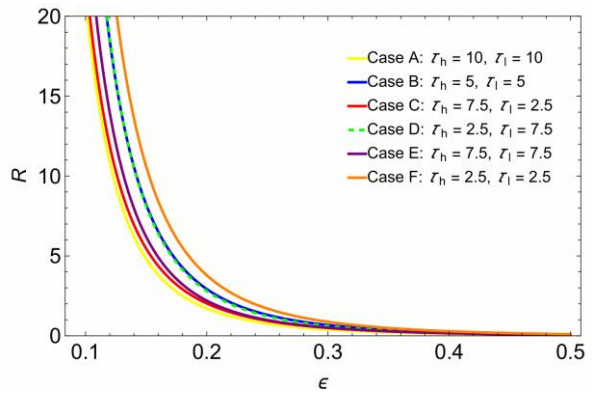

Figure 4 The cooling rate (R) as a function of the COP (ε) with various heating and cooling stroke times, in cases of : (A). $\tau_h = \tau_l = 10$; (B) $\tau_h = \tau_l = 5$; (C) $\tau_h = 7.5$, $\tau_l = 2.5$; (D) $\tau_h = 2.5$, $\tau_l = 7.5$; (E) $\tau_h = 7.5$, $\tau_l = 7.5$; and (F) $\tau_h = 2.5$, $\tau_l = 2.5$

Since internal dissipation is neglected, irreversibility in the present model arises solely from finite-time heat exchange during the isochoric heating and cooling strokes. However, in this study we only consider the total entropy change of the working medium during one complete cycle which can be expressed as $\Delta S_{total} = \Delta S_{heating} + \Delta S_{cooling}$. Each entropy change during the isochoric strokes is given by:

$$\Delta S_{heating} = \frac{5}{2} k_B \left(\frac{m k_B}{2\pi\hbar^2}\right)^{3/2} \zeta\left(\frac{5}{2}\right) V_l \left[\left((T_2 - T_h)e^{-\alpha_h \tau_h} + T_h\right)^{3/2} - T_2^{3/2}\right], \tag{28}$$

and

$$\Delta S_{cooling} = \frac{5}{2} k_B \left(\frac{m k_B}{2\pi\hbar^2}\right)^{3/2} \zeta\left(\frac{5}{2}\right) V_h \left[\left((T_4 - T_l)e^{-\alpha_l \tau_l} + T_l\right)^{3/2} - T_4^{3/2}\right]. \tag{29}$$

The entropy change during the heating process is positive because heat is absorbed from the hot reservoir, while the entropy change during the cooling process is negative because heat is released to the cold reservoir (Zettira et al., 2024b). The total entropy change during the heating and cooling processes depends strongly on the thermal contact durations of each process. Figure 5 (a) illustrates the case where $\tau_l > \tau_h$, meaning the system spends more time in thermal contact with the cold reservoir than with the hot one. This configuration results in a negative total entropy change, indicating that the entropy lost during the cooling process exceeds the entropy gained during heating. Physically, this implies that heat is released to the cold reservoir under more reversible conditions, leading to reduced the entropy change from the perspective of the working substance, but remains non-negative for the overall system. This configuration is thermodynamically favorable and supports enhanced performance of the refrigeration cycle.

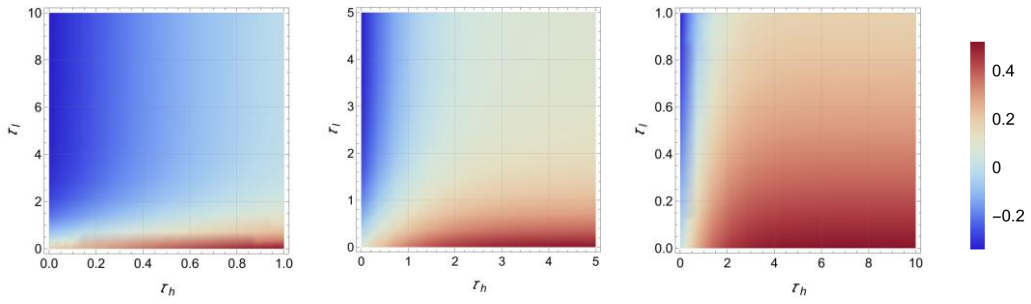

(a) (b) (c)

Figure 5 The entropy change as a function of heating τ_h (horizontal axis) and cooling τ_l (vertical axis) stroke time, in the cases of: (a) $\tau_l = 10, \tau_h = 1$; (b) $\tau_l = \tau_h = 5$; and (c) $\tau_l = 1, \tau_h = 10$, with a compression ratio $\kappa = 2$ and reservoirs temperatures $T_h = 45\ nK$ and $T_l = 20\ nK$.

In contrast, Figure 5 (c) shows the scenario where $\tau_h > \tau_l$, allowing the system more time to absorb heat from the hot reservoir. This leads to a positive total entropy change, meaning the entropy gained during heating is greater than the entropy lost during cooling. The longer heating duration enables a more irreversible heat exchange, while the shorter cooling time limits entropy dissipation to the environment. Since the heating process is excessively prolonged, the system fails to compensate for the associated entropy increase, leading to suboptimal cooling performance. Lastly, Figure 5 (b) presents a more balanced contour distribution, with a diagonal gradient transitioning from blue to red. The central area, shown in light gray, corresponds to conditions where the entropy change is close to zero. This corresponds to an optimal operating point, where the system undergoes nearly reversible heat exchange between the hot and cold reservoirs. In the context of cooling performance, this point is crucial, as it marks the regime where entropy change is minimized, allowing both efficiency and power to be simultaneously optimized.

5. CONCLUSION

This study demonstrates that the cooling performance of a bosonic-based quantum Otto refrigerator is strongly influenced by the balance between heating and cooling durations. When the thermalization times with the hot and cold reservoirs are symmetric, the cooling rate remains stable within a moderate range of COP values due to compensation in entropy production. In contrast, under partial thermalization, both the cooling rate and output power exhibit significant variations. Longer cooling periods combined with shorter heating times enhance both the cooling rate and COP by enabling more effective heat absorption from the cold reservoir, reducing entropy production, and shortening the overall cycle time. Conversely, extended heating with limited cooling increases entropy production and lowers the cooling rate, although high COP values can still be achieved. This behavior is linked to the population of excited atoms, which governs the energy exchange mechanism; higher heating temperatures allow more atoms to occupy excited states, thereby improving energy transfer and overall cooling performance. These findings provide insight into the optimization of finite-time quantum refrigeration cycles and may guide the design of controllable cooling protocols in bosonic quantum platforms. Future studies may extend this framework by incorporating particle interactions, internal dissipation, and non-ideal control processes to better approximate realistic experimental conditions.

ACKNOWLEDGEMENT

The Authors gratefully acknowledge the financial support provided by Universitas Andalas through the research grant Penelitian Skripsi Sarjana Batch I with contract No. 332/UN16.19/PT.01.03/PSS/2025

REFERENCE

Abah, O., & Lutz, E. (2016). Optimal performance of a quantum Otto refrigerator. *Europhysics Letters*, *113*(6), 60002.

Abah, O., Paternostro, M., & Lutz, E. (2020). Shortcut-to-adiabaticity quantum Otto refrigerator. *Physical Review Research*, *2*(2), 23120.

Altintas, F. (2025). Construction of a quantum Carnot refrigerator for general working substances. *The European Physical Journal Plus*, *140*(5), 379.

Aveline, D. C., Williams, J. R., Elliott, E. R., Dutenhoffer, C., Kellogg, J. R., Kohel, J. M., Lay, N. E., Oudrhiri, K., Shotwell, R. F., & Yu, N. (2020). Observation of Bose–Einstein condensates in an Earth-orbiting research lab. *Nature*, *582*(7811), 193–197.

Bagnato, V., Pritchard, D. E., & Kleppner, D. (1987). Bose-Einstein condensation in an external potential. *Physical Review A*, *35*(10), 4354.

Behzadi, N. (2024). Refrigeration by modified Otto cycles and modified swaps through generalized measurements. *Journal of Physics A: Mathematical and Theoretical*, *57*(29), 295308.

Belfaqih, I. H., Sutantyo, T. E. P., Prayitno, T. B., & Sulaksono, A. (2015). Quantum-Carnot engine for particle confined to 2D symmetric potential well. *AIP Conference Proceedings*, *1677*(1).

Bhandari, B., & Jordan, A. N. (2021). Minimal two-body quantum absorption refrigerator. *Physical Review B*, *104*(7), 75442.

Camati, P. A., Santos, J. F. G., & Serra, R. M. (2020). Employing non-Markovian effects to improve the performance of a quantum Otto refrigerator. *Physical Review A*, *102*(1), 12217.

Çengel, Y. A. (2008). *Thermodynamics : an Engineering Approach*. McGraw-Hill Higher Education.

Chen, J.-F., Sun, C.-P., & Dong, H. (2019). Boosting the performance of quantum Otto heat engines. *Physical Review E*, *100*(3), 32144.

Chen, J.-F., Sun, C. P., & Dong, H. (2021). Extrapolating the thermodynamic length with finite-time measurements. *Physical Review E*, *104*(3), 34117.

Cleri, F. (2024). Quantum computers, quantum computing, and quantum thermodynamics. *Frontiers in Quantum Science and Technology*, *3*, 1422257.

Contreras-Vergara, O., Valencia-Ortega, G., Sánchez-Salas, N., & Jiménez-Aquino, J. I. (2024). Performance at maximum figure of merit for a Brownian Carnot refrigerator. *Physical Review E*, *110*(2), 24123.

Cruz, C., Rastegar-Sedehi, H.-R., Anka, M. F., de Oliveira, T. R., & Reis, M. (2023). Quantum Stirling engine based on dinuclear metal complexes. *Quantum Science and Technology*, *8*(3), 35010.

Curzon, F. L., & Ahlborn, B. (1975). Efficiency of a Carnot engine at maximum power output. *American Journal of Physics*, *43*(1), 22–24.

Deffner, S., & Campbell, S. (2019). *Quantum Thermodynamics: An introduction to the thermodynamics of quantum information*. Morgan & Claypool Publishers.

Fahriza, A., Sutantyo, T. E. P., & Abdullah, Z. (2022). Optimizations of multilevel quantum engine with N noninteracting fermions based on Lenoir cycle. *The European Physical Journal Plus*, *137*(9), 1030.

Fei, Z., Chen, J.-F., & Ma, Y.-H. (2022). Efficiency statistics of a quantum Otto cycle. *Physical Review A*, *105*(2), 22609.

Getie, M. Z., Lanzetta, F., Bégot, S., Admassu, B. T., & Hassen, A. A. (2020). Reversed regenerative Stirling cycle machine for refrigeration application: A review. *International Journal of Refrigeration*, *118*, 173–187.

Griffiths, D. J., & Schroeter, D. F. (2018). *Introduction to quantum mechanics*. Cambridge university press.

He, Y., Ge, Y., Chen, L., & Feng, H. (2025). Exergy-based efficient ecological-function optimization for endoreversible Carnot refrigerators. *Journal of Non-Equilibrium Thermodynamics*, *0*.

Hu, H., Yu, Z.-Q., Wang, J., & Liu, X.-J. (2021). First-order Bose-Einstein condensation with three-body interacting bosons. *Physical Review A*, *104*(4), 43301.

Jiao, G., Xiao, Y., He, J., Ma, Y., & Wang, J. (2021). Quantum Otto refrigerators in finite-time cycle period. *New Journal of Physics*, *23*(6), 63075.

Kaur, K., Rebari, S., & Singh, V. (2025). Performance analysis of quantum harmonic Otto engine and refrigerator under a trade-off figure of merit. *Journal of Non-Equilibrium Thermodynamics*, *50*(1), 1–19.

Kurniasih, N., Kusmiyati, M., Nurhasnah, Puspita Sari, R., & Wafdan, R. (2019). Potensi Daun Sirsak (Annona muricata Linn), Daun Binahong (Anredera cordifolia (Ten) Steenis), dan Daun Benalu Mangga (Dendrophthoe pentandra) Sebagai Antioksidan Pencegah Kanker. *Jurnal Istek*, *9*(1), 162–184.

Long, R., & Liu, W. (2015). Performance of quantum Otto refrigerators with squeezing. *Physical Review E*, *91*(6), 62137.

Manikandan, S. K., Jussiau, É., & Jordan, A. N. (2020). Autonomous quantum absorption refrigerators. *Physical Review B*, *102*(23), 235427.

Maslennikov, G., Ding, S., Hablützel, R., Gan, J., Roulet, A., Nimmrichter, S., Dai, J., Scarani, V., & Matsukevich, D. (2019). Quantum absorption refrigerator with trapped ions. *Nature Communications*, *10*(1), 202.

Mohanraj, M., & Abraham, J. D. A. P. (2022). Environment friendly refrigerant options for automobile air conditioners: a review. *Journal of Thermal Analysis and Calorimetry*, *147*(1), 47–72.

Mohapatra, A., Prusty, A. K., Nanda, J., Das, S. N., & Pandey, H. (2021). Potential Refrigerants and Their Effect on the Environment—A Review. *Current Advances in Mechanical Engineering: Select Proceedings of ICRAMERD 2020*, 239–249.

Myers, N. M., Peña, F. J., Negrete, O., Vargas, P., De Chiara, G., & Deffner, S. (2022a). Boosting engine performance with Bose–Einstein condensation. *New Journal of Physics*, *24*(2), 25001.

Myers, N. M., Abah, O., & Deffner, S. (2022b). Quantum thermodynamic devices: From theoretical proposals to experimental reality. *AVS Quantum Science*, *4*(2).

Nolte, D. D. (2019). *Introduction to Modern Dynamics: Chaos, Networks, Space, and Time*. Oxford University

Press. https://doi.org/10.1093/oso/9780198844624.001.0001

Pathria, R. K., & Beale, P. D. (2011a). 1-the statistical basis of thermodynamics. *Statistical Mechanics*, 1–23.

Pathria, R. K., & Beale, P. D. (2011b). 15 - Fluctuations and Nonequilibrium Statistical Mechanics. In R. K. Pathria & P. D. Beale (Eds.), *Statistical Mechanics (Third Edition)* (Third Edit, pp. 583–635). Academic Press. https://doi.org/https://doi.org/10.1016/B978-0-12-382188-1.00015-3

Raja, S. H., Maniscalco, S., Paraoanu, G.-S., Pekola, J. P., & Gullo, N. Lo. (2021). Finite-time quantum Stirling heat engine. *New Journal of Physics*, *23*(3), 33034.

Savitha, D. C., Ranjith, P. K., Talawar, B., & Rana Pratap Reddy, N. (2022). Refrigerants for sustainable environment–a literature review. *International Journal of Sustainable Energy*, *41*(3), 235–256.

Singh, S., & Abah, O. (2020). Energy optimization of two-level quantum Otto machines. *ArXiv Preprint ArXiv:2008.05002*.

Singh, V., Singh, S., Abah, O., & Müstecaplıoğlu, Ö. E. (2022). Unified trade-off optimization of quantum harmonic Otto engine and refrigerator. *Physical Review E*, *106*(2), 24137.

Sutantyo, T. (2020). Three-State Quantum Heat Engine Based on Carnot Cycle. *Jurnal Fisika Unand*, *9*, 142–149. https://doi.org/10.25077/jfu.9.1.142-149.2020

Sutantyo, T. E. P., Zettira, Z., Fahriza, A., & Abdullah, Z. (2024). Performance of 3D quantum Otto engine with partial thermalization. *Journal of Physics: Conference Series*, *2734*(1), 12031.

Sutantyo, T. E. P., Belfaqih, I. H., & Prayitno, T. B. (2015). Quantum-Carnot engine for particle confined to cubic potential. *AIP Conference Proceedings*, *1677*(1), 40011.

Velasco, S., Roco, J. M. M., Medina, A., & Hernández, A. C. (1997). New performance bounds for a finite-time carnot refrigerator. *Physical Review Letters*, *78*(17), 3241.

Wiedmann, M., Stockburger, J. T., & Ankerhold, J. (2021). Non-Markovian quantum Otto refrigerator: Dynamical operation through finite-time thermal coupling. *The European Physical Journal Special Topics*, *230*(4), 851–857.

Xu, Y., Ruan, H., Luo, S., Guo, S., He, X., & Wang, J. (2025). Enhancing Otto refrigerator performance with a precooling strategy. *Physical Review E*, *111*(2), L022101.

Yin, Y., Chen, L., & Wu, F. (2017). Optimal power and efficiency of quantum Stirling heat engines. *The European Physical Journal Plus*, *132*, 1–10.

Zettili, N. (2009). *Quantum mechanics: concepts and applications*.

Zettira, Z., Sutantyo, T. E. P., & Abdullah, Z. (2024a). Efficiency at Maximum Power of Endoreversible Quantum Otto Engine with Partial Thermalization in 3D Harmonic Potential. *JURNAL ILMU FISIKA| UNIVERSITAS ANDALAS*, *16*(1), 22–33.

Zettira, Z., Fahriza, A., Sutantyo, T. E. P., & Abdullah, Z. (2024b). Enhancing quantum Otto engine performance in generalized external potential on Bose–Einstein condensation regime. *The European Physical Journal Plus*, *139*(3), 282.

Zhang, Y. (2020). Optimization performance of quantum Otto heat engines and refrigerators with squeezed thermal reservoirs. *Physica A: Statistical Mechanics and Its Applications*, *559*, 125083.

Zhang, Z., Su, H., Dai, G., Li, X., & Zeng, L. (2023). Effects of variable-temperature heat reservoirs on performance of irreversible Carnot refrigerator with heat recovery. *Scientific Reports*, *13*(1), 23068.